A nanoscale pn junction in series with tunable Schottky barriers

Lee Aspitarte, Daniel R. McCulley, and Ethan D. Minot[a)]
Department of Physics, Oregon State University, Corvallis, Oregon 97331, USA

PN junctions in nanoscale materials are of interest for a range of technologies including photodetectors, solar cells, and light-emitting diodes. However, Schottky barriers at the interface between metal contacts and the nanomaterial are often unavoidable. The effect of metal-semiconductor interfaces on the behavior of nanoscale diodes must be understood, both to extract the characteristics of the pn junction, and to understand the overall characteristics of the final device. Here, we study the current-voltage characteristics of diodes that are formed in fully suspended carbon nanotubes (CNTs). We utilize tunable Schottky barrier heights at the CNT-metal interface to elucidate the role of the Schottky barriers on the device characteristics. We develop a quantitative model to show how a variety of device characteristics can arise from apparently similar devices. Using our model we extract key parameters of the Schottky barriers and the pn junction, and predict the overall I-V characteristics of the device. Our equivalent circuit model is relevant to a variety of nanomaterial-based diode devices that are currently under investigation. *Published by AIP Publishing.* [http://dx.doi.org/10.1063/1.4994194]

INTRODUCTION

The pn junction is a crucial building block for modern electronics and optoelectronics. Researchers have recently created and studied pn junctions in a variety of nanoscale semiconducting materials, including carbon nanotubes (CNTs)[1] and transition metal dichalcogenides (reviewed in Ref. [2]). These nanomaterial-based pn junctions are being investigated for their potential applications as rectifying diodes, solar cells, photodetectors, and light-emitting diodes (LEDs).

Measurements of pn junctions in nanomaterials are often complicated by metal-semiconductor contacts. Previous work has shown that Schottky barriers associated with metal-semiconductor contacts drastically affect the electrical characteristics of nanomaterial-based field-effect transistors.[3–5] However, the effect of Schottky barriers on the electrical characteristics of nanomaterial-based diodes is relatively unexplored. For example, CNT diode devices have been reported with a diversity of electrical characteristics that cannot be accounted for by a simple pn junction.[6,7] In this work, we elucidate the role of Schottky barriers in lateral pn-junction devices made from individual suspended carbon nanotubes. We vary the Schottky barrier heights (SBHs) and establish the effect of Schottky contacts on the overall properties of the nanoscale diode.

We have chosen suspended CNTs with dual gates as our model system [Fig. 1(a)]. Dual-gated CNTs have received considerable attention in recent years, due to their promising electronic and optoelectronic characteristics.[7–16] Fully suspended dual-gated CNTs are an ideal model system for exploring the role of Schottky contacts on nanoscale diodes. First, the fully suspended CNT is a "clean" system. There are no complications associated with substrate-induced

disorder, doping, or screening.[17] Second, we can characterize the diameter and chirality of the CNT under study,[15] allowing precise comparison between device characteristics and electronic structure. Third, our device geometry creates Schottky barriers that are sufficiently long (>100 nm) so that transport past the barrier is via thermionic emission, rather than a complicated mixture of tunneling and thermionic emission.[3,4] Last, the SBH is tunable. The work function (WF) of the metal contacts changes gradually when the device is transferred from laboratory air to a vacuum environment. Previous authors have used this effect to study the role of SBH on CNT field-effect transistors (CNT FETs),[18,19] and here we use the effect for the first time to study the role of SBH on a nanomaterial-based diode.

METHODS

Ultra-clean suspended CNTs were fabricated by growing CNTs over pre-made electrode structures. Electrodes were fabricated on 4-in. Si/SiO_2 wafers (500 nm oxide layer). First, the pair of gate electrodes was patterned and deposited (W/Pt 5 nm/60 nm). The separation distance between gate electrodes is 200 nm. The gate electrodes were then buried by SiO_2 (800 nm thickness) and source/drain electrode pairs were patterned and deposited (W/Pt 5 nm/60 nm). The separation distance between source and drain electrodes is 2 μm. Reactive-ion etching was used to make a 700-nm-deep trench between the source and drain electrodes. The source and drain electrodes serve as an etch mask to define the edge of the trench. CNT growth catalyst (1 nm Ti/20 nm SiO_2/ 1 nm Fe) was patterned and deposited on top of the source and drain electrodes. CNTs were grown using chemical vapor deposition in a tube furnace at 800 °C. The chips were shuttled in/out of the furnace hot zone to minimize heat exposure. The growth recipe consists of a 1 min 1 SLM H_2 anneal followed by a 5 min growth phase with 0.15 SLM

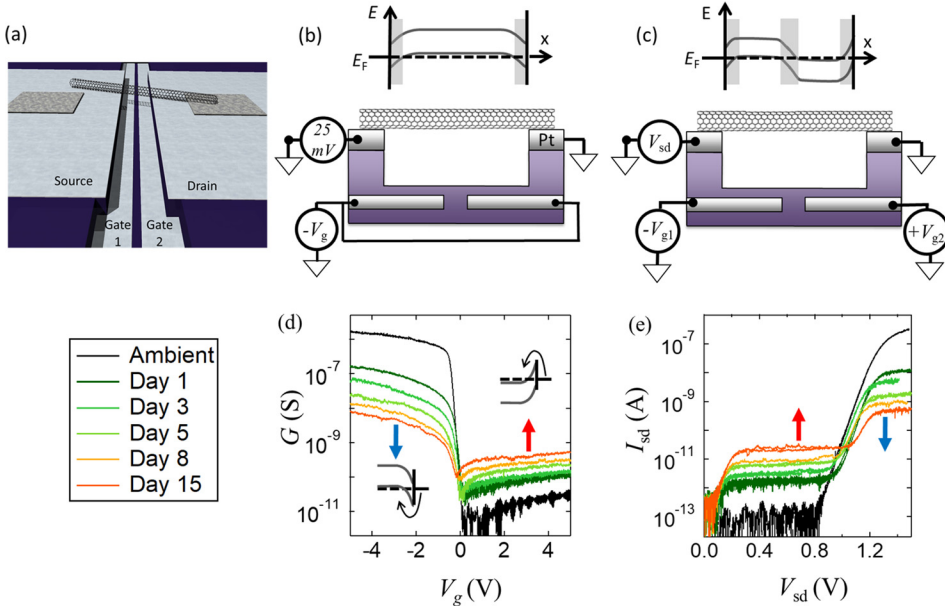a)Author to whom correspondence should be addressed: ethan.minot@oregonstate.edu

FIG. 1. Comparison of the CNT FET characteristics and the CNT diode characteristics. (a) Schematic diagram of the device geometry. All dimensions are to scale except for the CNT. (b) Cross-sectional diagram and band diagram for the device when operated as a CNT FET. (c) Device schematic and band diagram for the device when operated as a diode. (d) Conductance of the CNT FET measured with $V_{sd} = 25$ mV. The black curve is measured in laboratory air. The color of the curves changes from dark green to orange as the device is left in vacuum for two weeks. All measurements are taken at $T = 295$ K. (e) CNT diode characteristics measured at $V_{g1} = -V_{g2} = -5$ V over the same time period.

ethanol, 0.3 SLM methanol, and 0.45 SLM H_2. The ethanol and methanol are introduced into Ar gas with a bubbler.

After device fabrication, electrode pairs that are connected by individual CNTs were identified by electrical characterization and scanning photocurrent microscopy. Spectrally resolved photocurrent was used to determine the diameter and chirality of the CNT under study.[15]

RESULTS AND DISCUSSION

We first verify the role of the SBH on the transport characteristics of a suspended CNT FET. Figure 1(d) shows the measured $G(V_g)$ of a dual-gated suspended CNT. The CNT chiral index is (29, 10) which corresponds to a diameter of 2.74 nm and an S_{11} optical resonance energy of 430 meV (see Fig. S2, supplementary material). To perform field-effect transistor measurements, the gates are configured such that $V_{g1} = V_{g2}$. A variety of SBHs were achieved by transferring the device from laboratory air to vacuum. Measurements were performed in vacuum over the course of 2 weeks. Consistent with the previous literature, the p-type conductivity of the CNT FET decreases as a function of time spent in vacuum, while the n-type conductivity increases [Fig. 1(d)].[15] The n-type and p-type conductivities are related to the electron SBH, Φ_e, and the hole SBH, Φ_h, respectively [Fig. 1(d), inset]. As previously explained by McClain et al.,[18] a reduction in metal WF over time leads to a decrease in Φ_e and increase in Φ_h, consistent with our transport measurements. In a material with a homogeneous transport band gap E_g, we expect $\Phi_h + \Phi_e$ to equal the bandgap; therefore, a decrease in Φ_e will be balanced by an increase in Φ_h.

The diode characteristics of the same CNT device were measured as the metal WF was varied [Fig. 1(e)]. After each field-effect transistor measurement, the gates were reconfigured such that $V_{g1} = -V_{g2} = -5$ V. Figure 1(e) shows the resulting I_{sd}–V_{sd} characteristics for $V_{sd} > 0$. In reverse bias (not shown) the current is below the noise floor of our current amplifier [$|I| < 10^{-13}$ A, see Fig. S1(a), supplementary material]. In ambient environment (black

curve), the forward-biased current remains below the noise floor of our measurement for $V_{sd} < 0.8$ V. For $V_{sd} > 0.8$ V, the current increases exponentially before finally rolling off into a linear I_{sd}–V_{sd} relationship. After a day in vacuum (dark green curve), the device characteristics dramatically change. Unlike a conventional diode, we observe two regimes where the current exponentially increases and two regimes where the current plateaus. The first exponential increase begins near $V_{sd} = 0$ V. The voltage threshold for the second exponential increase is variable, changing with the number of days in vacuum [Fig. 1(e)], and with the magnitude of the applied gate voltages [see supplementary material, Fig. S1(b)]. As the device sits in vacuum over the course of two weeks, the current level of the first plateau increases, while the current level of the second plateau decreases.

We have developed an equivalent circuit model that explains the observed diode characteristics. As shown in Fig. 2(a), the pn junction in the center of the CNT is in series with two reverse-biased Schottky diodes. One Schottky diode is associated with the junction between the source electrode and the p-doped section of CNT. The other Schottky diode is associated with the junction between the drain electrode and the n-doped section of CNT. We assume that majority charge carriers thermalize in the sections of CNT connecting the three circuit elements. In our model, the current plateaus correspond to the saturation currents of the Schottky diodes [Fig. 2(d), regions labeled R2 and R4]. The pn junction determines the current before the first plateau and in-between the plateaus [Fig. 2(d), regions labeled R1 and R3]. We now formalize this model and quantify the key parameters for the device shown in Fig. 1(e).

The source-drain bias V_{sd}, is distributed across the three circuit elements shown in Fig. 2(a) such that

$$V_{sd} = V_{SBh} + V_{pn} + V_{SBe}. \qquad (1)$$

The current through each circuit element must be equal, yielding the condition $I_{sd} = I_{SBh} = I_{pn} = I_{SBe}$. Thus, I_{sd} is constrained by the coupled equations
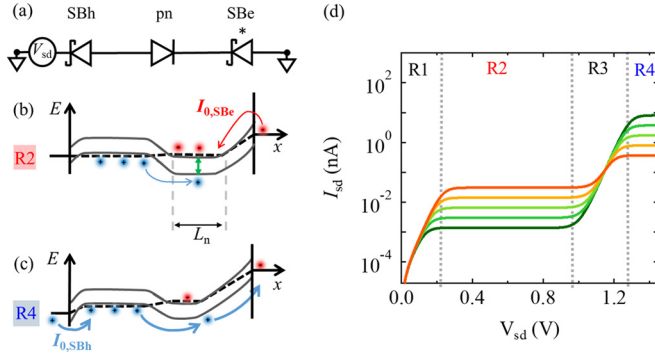
FIG. 2. (a) Equivalent circuit for the suspended CNT pn junction. (b) and (c) Schematic band diagrams along the axis of the CNT for the regimes R2 and R4 as labeled in part d. (d) Simulated I_{sd}-V_{sd} characteristic that closely match Fig. 1(e). The SBH heights are varied from $\Phi_e = 250\,\mathrm{meV}$ (dark green) to $\Phi_e = 170\,\mathrm{meV}$ (orange), maintaining $\Phi_e + \Phi_h = 410\,\mathrm{meV}$. Other free parameters are fixed: $\tau_h = 1$, $\tau_e = 5.5 \times 10^{-3}$, $\tau_{pn} = 1$, $n = 1.3$, $E_g = 500\,\mathrm{meV}$, and $V_{shift} = 0.9\,\mathrm{V}$.

$$I_{SBh} = I_{0,SBh}\left(1 - e^{-\frac{eV_{SBh}}{k_B T}}\right), \tag{2}$$

$$I_{pn} = I_{0,pn}\left(e^{\frac{eV_{pn}}{n k_B T}} - 1\right), \tag{3}$$

$$I_{SBe} = \begin{cases} I_{0,SBe}\left(1 - e^{-\frac{eV_{SBe}}{k_B T}}\right), & V_{SBe} < V_{shift} \\ G_0(V_{SBe} - V_{shift}), & V_{SBe} > V_{shift} \end{cases} \tag{4a,b}$$

where $I_{0,SBh}$, $I_{0,pn}$, and $I_{0,SBe}$ are the saturation currents of the respective diodes, n is the ideality factor of the pn junction, G_0 is the conductance quantum, and V_{shift} is a critical voltage at which the transport mechanism changes for I_{SBe}. Equations (2) and (4a) are flipped in sign compared to a conventional Schottky diode due to the reversed orientation.

The piecewise function [Eq. (4)] describes an unusual voltage dependence of I_{SBe}. A mechanism for this voltage-triggered change was proposed by Liu et al.[7] The length of the n-doped region L_n, becomes smaller as V_{SBe} is increased. When L_n is sufficiently short ($V_{SBe} > V_{shift}$), holes are transmitted directly from the p-doped region to the drain electrode without recombination [Fig. 2(c)]. In this regime, the hole current bypasses the Schottky barrier for electrons.

To complete our model, we consider the factors influencing the saturation currents $I_{0,SBh}$, $I_{0,pn}$, and $I_{0,SBe}$. Using a 1-D Landauer formalism for electron transport in a CNT, Bosnick et al. calcuated[20]

$$I_{0,pn} = \frac{8 e k_B}{h} \tau_{pn} T e^{-\frac{E_g}{k_B T}}, \tag{5}$$

where τ_{pn} is the transmission coefficient over the pn junction and E_g is the bandgap of the CNT at the location of the pn junction ($E_g \gg k_B T$). Applying the same approach to a 1-D Schottky contact yields

$$I_{0,SBh} = \frac{4 e k_B}{h} \tau_h T e^{-\frac{\Phi_h}{k_B T}}, \tag{6}$$

$$I_{0,SBe} = \frac{4 e k_B}{h} \tau_e T e^{-\frac{\Phi_e}{k_B T}}, \tag{7}$$

where Φ_h and Φ_e are the Schottky barrier heights for holes and electrons, respectively, and τ_h and τ_h are the transmission coefficients across the two Schottky barriers. Equations

(6) and (7) are consistent with the 1D Richardson constant formalism previously used to analyze CNT 1D contacts.[4,21]

Figure 2(d) shows solutions to the coupled set of equations, Eqs. (1)–(4). These curves were generated by determining the voltage drop across each circuit element for a given I_{sd}, (see supplementary material note 1). The free parameters τ_h, τ_e, τ_{pn}, n, E_g, and V_{shift} are the same for all 5 curves and we constrain $\Phi_h + \Phi_e = 410\,\mathrm{meV}$, as discussed further below. The simulated device characteristics [Fig. 2(d)] are in excellent agreement with our measurements [Fig. 1(e)].

It is instructive to qualitatively describe the features of Fig. 2(d). The four distinct regimes of $I_{sd}(V_{sd})$ are labeled in Fig. 2(d) as R1, R2, R3, and R4. In R1, the current-limiting circuit element is the pn junction. This can be understood by calculating the zero-bias conductance of each circuit element. We expect the pn junction to have the smallest zero bias conductance because E_g is greater than either Φ_h or Φ_e, and therefore, $I_{0,pn}$ is much less than $I_{0,SBh}$ or $I_{0,SBe}$. In R2, the current-limiting circuit element is the reverse-biased Schottky barrier for electrons and the current plateau occurs at $I_{0,SBe}$. In R3, the Schottky barrier for electrons is by-passed, and the current-limiting circuit element is the pn junction. Finally, in R4, the current-limiting circuit element is the reverse-biased Schottky barrier for holes and the current plateau occurs at $I_{0,SBh}$.

Temperature-dependent measurements are useful for testing our model and for constraining the model parameters. Figure 3(a) shows measurements of the diode characteristics on Day 15 ($V_{g1} = -V_{g2} = -5\,\mathrm{V}$) as the temperature T, is varied from $300\,\mathrm{K}$ to $200\,\mathrm{K}$ in steps of $25\,\mathrm{K}$. The current at the plateaus is exponentially suppressed as T is lowered. From our equivalent circuit model we associate the first plateau with $I_{0,SBe}$ and the second plateau with $I_{0,SBh}$. As shown in Fig. 3(b), the exponential suppression of $I_{0,SBe}$ and $I_{0,SBh}$ agrees with the predictions of Eqs. (6) and (7). Using Eqs. (6) and (7) to fit the temperature dependence of the current plateaus we find $\Phi_e = 192 \pm 14\,\mathrm{meV}$, $\Phi_h = 219 \pm 24\,\mathrm{meV}$ and $2.7 \times 10^{-3} < \tau_e < 1.1 \times 10^{-2}$ and $0.4 < \tau_h < 3.9$.

Our electrical measurements give a quantitative estimate of $\Phi_e + \Phi_h \approx 410\,\mathrm{meV}$, which we now compare to the CNT chiral index. The chiral index of this CNT is $(n, m) = (29, 10)$ which has a lowest-energy exciton resonance $S_{11} = 430\,\mathrm{meV}$ (see Fig. S2, supplementary material). Within experimental uncertainty, S_{11} is equal to our electronic measurement $\Phi_e + \Phi_h = 410 \pm 30\,\mathrm{meV}$. The equality between S_{11} and $\Phi_e + \Phi_h$ suggests that electron-electron interactions are strongly screened at the location where the Schottky barriers form. This is a reasonable assumption, because the Schottky barriers are in close proximity to the metal electrodes.

In contrast to the electrostatically screened environment near the metal electrodes, the pn junction is located in the center of the CNT, far from the metal electrodes. Previous experiments on CNT pn junctions,[22] scanning tunneling spectroscopy of CNTs,[23] and CNTs in dielectric environments,[24] suggest that E_g increases when screening is reduced. Therefore, we have considered the possibility that $E_g > \Phi_e + \Phi_h$. We achieve an excellent fit to our
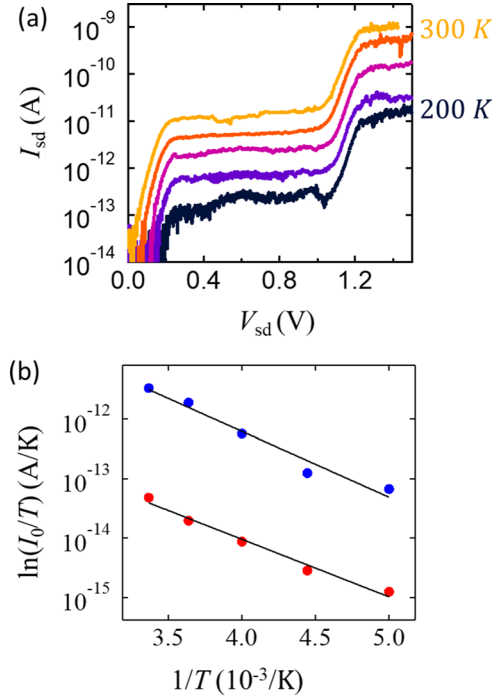
FIG. 3. Temperature dependent I_{sd}-V_{sd} characteristics. (a) Temperature dependent diode curves [same device as Fig. 1(e)]. (b) 1D Richardson plot of the first (red) and second (blue) current plateaus. Solid lines are fits to Eqs. (6) and (7). The extracted Schottky barrier heights are $\Phi_e = 192 \pm 14$ meV and $\Phi_h = 219 \pm 24$ meV.

experimental data by setting $\tau_{pn} = 1$ and $E_g = 500$ meV [Fig. 2(d)]. A transmission coefficient of order unity is a reasonable assumption because the expected scattering length in the suspended CNT is greater than the pn junction intrinsic region length.[25] We conclude that the I_{sd}–V_{sd} characteristics [Fig. 1(e)] are consistent with a growing body of evidence for a screening-dependent transport gap in CNTs.

Axial strain is a secondary factor that could cause discrepancy between the band gap at the pn junction and the sum $\Phi_e + \Phi_h$. There is a downward electrostatic force on the suspended CNT when V_g is non-zero. Previous nanoelectromechanical studies of suspended CNTs with similar geometry to our devices estimate an axial strain $\sigma \sim 0.02\%$ when $V_g = 10$ V.[26] Given the CNT chiral index (29, 10), we expect $dE_g/d\sigma \sim 50$ meV per %.[27,28] Thus, the expected strain-induced change in band gap (~ 1 meV) is too small to explain a 70 meV discrepancy between E_g and the sum $\Phi_e + \Phi_h$.

Our discussion, so far, has focused on I_{sd}–V_{sd} characteristics in vacuum (day 1–15). We now comment on the I_{sd}–V_{sd} characteristics in an ambient environment [black curve, Fig. 1(e)]. In an ambient environment, the WF is sufficiently large to form Ohmic p-type contacts i.e., $\Phi_h \approx 0$ and $\Phi_e \approx E_g$. In this situation, $I_{0,SBe}$ is below the noise floor of our measurement (showing that $\Phi_e > 320$ meV), and $I_{0,SBh}$ exceeds 200 nA (showing that $\Phi_h < 80$ meV). In addition, because the p-type contact is Ohmic, the current linearly increases beyond regime R3, instead of plateauing. This linearly increasing current can be described by replacing the p-type Schottky diode of the equivalent circuit of Fig. 2(a) with a series resistor.[29]

Our quantitative model of the nanoscale diode device shows how a variety of device characteristics can arise from apparently similar devices. The work function of the metal contacts, the band gap of the CNT, and the transmission coefficients all strongly affect the device characteristics. We have measured over 20 suspended CNT diode devices and the various characteristics that we have observed are explained within the framework described here.

CONCLUSION

In conclusion, our experiments on suspended CNT diodes reveal regimes in which I_{sd} is limited by the pn junction, but other regimes where I_{sd} is limited by the Schottky barriers at the metal-semiconductor contacts. The p-type and n-type SBHs are determined by analyzing temperature dependent measurements. We develop a quantitative model for the transport characteristics of the pn junction in series with reverse-biased Schottky diodes. Our model explains the wide range of I_{sd}–V_{sd} characteristics observed in suspended CNT diodes. Key features of our equivalent circuit model are relevant to the variety of nanomaterial-based diode devices that are currently under investigation for solar cell, photodetector and LED applications.

SUPPLEMENTARY MATERIAL

See supplementary material for a description of the equations and parameters used to generate Fig. 3(d); reverse bias measurements of the CNT diode featured in Fig. 1.; diode characteristics at various values of V_{g1} and V_{g2}; photocurrent spectroscopy of the CNT diode featured in Fig. 1.

ACKNOWLEDGMENTS

[1]J. U. Lee, P. P. Gipp, and C. M. Heller, Appl. Phys. Lett. **85**, 145 (2004).
[2]K. Mak and J. Shan, Nat. Photonics **10**, 216 (2016).
[3]A. Allain, J. Kang, K. Banerjee, and A. Kis, Nat. Mater. **14**, 1195 (2015).
[4]J. Svensson and E. E. B. Campbell, J. Appl. Phys. **110**, 111101 (2011).
[5]Y. Xu, C. Cheng, S. Du, J. Yang, B. Yu, J. Luo, W. Yin, E. Li, S. Dong, P. Ye, and X. Duan, ACS Nano **10**, 4895 (2016).
[6]S. W. Chang, K. Bergemann, R. Dhall, J. Zimmerman, S. Forrest, and S. B. Cronin, IEEE Trans. Nanotechnol. **13**, 41 (2014).
[7]C. H. Liu, C. C. Wu, and Z. Zhong, Nano Lett. **11**, 1782 (2011).
[8]N. M. Gabor, Z. Zhong, K. Bosnick, J. Park, and P. L. McEuen, Science **325**, 1367 (2009).
[9]A. Malapanis, V. Perebeinos, D. P. Sinha, E. Comfort, and J. U. Lee, Nano Lett. **13**, 3531 (2013).
[10]P. Dhakras and J. U. Lee, Appl. Phys. Lett. **109**, 203114 (2016).
[11]S.-W. Chang, J. Theiss, J. Hazra, M. Aykol, R. Kapadia, and S. B. Cronin, Appl. Phys. Lett. **107**, 53107 (2015).
[12]S. W. Chang, J. Hazra, M. Amer, R. Kapadia, and S. B. Cronin, ACS Nano **9**, 11551 (2015).
[13]M. Barkelid and V. Zwiller, Nat. Photonics **8**, 47 (2013).
[14]M. Barkelid and V. Zwiller, J. Appl. Phys. **114**, 164320 (2013).
[15]L. Aspitarte, D. R. McCulley, and E. D. Minot, Nano Lett. **16**, 5589 (2016).
[16]G. Buchs, S. Bagiante, and G. A. Steele, Nat. Commun. **5**, 4987 (2014).
[17]E. A. Laird, F. Kuemmeth, G. A. Steele, K. Grove-Rasmussen, J. Nygård, K. Flensberg, and L. P. Kouwenhoven, Rev. Mod. Phys. **87**, 703 (2015).
[18]D. McClain, N. Thomas, S. Youkey, R. Schaller, J. Jiao, and K. P. O'Brien, Carbon N. Y. **47**, 1493 (2009).

[19]S. Heinze, J. Tersoff, R. Martel, V. Derycke, J. Appenzeller, and P. Avouris, Phys. Rev. Lett. **89**, 106801 (2002).

[20]K. Bosnick, N. Gabor, and P. McEuen, Appl. Phys. Lett. **89**, 163121 (2006).

[21]J. Svensson, A. A. Sourab, Y. Tarakanov, D. S. Lee, S. J. Park, S. J. Baek, Y. W. Park, and E. E. B. Campbell, Nanotechnology **20**, 175204 (2009).

[22]E. Comfort and J. U. Lee, Sci. Rep. **6**, 28520 (2016).

[23]H. Lin, J. Lagoute, V. Repain, C. Chacon, Y. Girard, J.-S. Lauret, F. Ducastelle, A. Loiseau, and S. Rousset, Nat. Mater. **9**, 235 (2010).

[24]L. Aspitarte, D. R. McCulley, A. Bertoni, J. O. Island, M. Ostermann, M. Rontani, G. A. Steele, and E. D. Minot, Sci. Rep. **7**, 8828 (2017).

[25]M. S. Purewal, B. H. Hong, A. Ravi, B. Chandra, J. Hone, and P. Kim, Phys. Rev. Lett. **98**, 186808 (2007).

[26]V. A. Sazonova, "A tunable carbon nanotube resonator," Ph.D. thesis (Cornell University, 2006).

[27]E. D. Minot, Y. Yaish, V. Sazonova, J.-Y. Park, M. Brink, and P. L. McEuen, Phys. Rev. Lett. **90**, 156401 (2003).

[28]M. Huang, Y. Wu, B. Chandra, H. Yan, Y. Shan, T. F. Heinz, and J. Hone, Phys. Rev. Lett. **100**, 136803 (2008).

[29]G. Buchs, M. Barkelid, S. Bagiante, G. A. Steele, and V. Zwiller, J. Appl. Phys. **110**, 74308 (2011).